Infrared photodissociation spectra of $CH_3^+-Ar_n$ complexes ($n=1-8$)

Rouslan V. Olkhov, Sergey A. Nizkorodov, and Otto Dopfer[a)]
Institut für Physikalische Chemie, Universität Basel, Klingelbergstrasse 80, CH-4056, Switzerland

(Received 9 February 1998; accepted 19 March 1998)

Infrared photodissociation spectra of the ionic complexes $CH_3^+-Ar_n$ ($n=1-8$) have been recorded in the vicinity of the ν_3 asymmetric stretching vibration of the CH_3^+ monomer. The CH_3^+-Ar dimer has also been investigated in the spectral range of the first CH stretching overtones, resulting in the characterization of its $2\nu_1$, $\nu_1+\nu_3$, and $2\nu_3$ vibrational states at the level of rotational resolution. The spectrum of CH_3^+-Ar is consistent with a pyramidal C_{3v} minimum structure of the complex predicted by *ab initio* calculations at the MP2 level, whereby the Ar atom is attached to the empty $2p_z$ orbital of the CH_3^+ moiety. The rotationally resolved ν_3 spectrum of the $CH_3^+-Ar_2$ trimer indicates that the two Ar atoms are located on opposite sides of the CH_3^+ moiety on the C_3 axis, with significantly differing intermolecular C–Ar bond lengths. The splittings observed in the trimer spectrum are attributed to a tunneling motion between two equivalent C_{3v} minimum configurations via a symmetric D_{3h} transition state. The spectra of larger clusters ($n\geqslant 3$) lack rotational resolution, however the positions and profiles of the ν_3 band suggest that the additional Ar atoms are weakly attached to $CH_3^+-Ar_2$ trimer, which acts as the effective nucleation center for the cluster growth. The stretching fundamentals of the CH_3^+ ion core in the $CH_3^+-Ar_n$ clusters are intermediate between those of the methyl radical and the methyl cation, implying a substantial charge transfer from the rare gas atoms to the unoccupied $2p_z$ orbital of CH_3^+. © *1998 American Institute of Physics.* [S0021-9606(98)01524-4]

I. INTRODUCTION

The methyl radical and its cation belong to the group of the most important reactive species in organic, combustion, atmospheric, and interstellar chemistry.[1–8] Both molecules are ubiquitous components of various hydrocarbon-based discharges and plasmas.[9,10] The methyl and its homologous radicals are readily produced by photolysis of suitable organic precursor molecules. For example, UV photodissociation of CH_3I into CH_3+I represents a prototype photofragmentation reaction for polyatomic molecules.[11,12] The methyl cation is a very strong electrophilic agent,[13,14] capable of capturing electrons and functional groups from a variety of neutral organic molecules.[15–18] It even reacts with saturated hydrocarbons to produce more stable secondary and tertiary carbocations.[9,18–20] Because of their importance, both CH_3^+ and CH_3 have served as targets for numerous theoretical and experimental studies exploring their structural, reactive, and spectroscopic properties. Both possess a planar D_{3h} equilibrium geometry with only slightly differing C–H bond lengths ($r_e=1.076$ and 1.087 Å for CH_3 and CH_3^+, respectively).[12,20] The in-plane stretching and bending vibrational frequencies (ν_1,ν_3,ν_4) are similar or somewhat lower in the ion compared to the radical (Table I), whereas the frequency for the out-of-plane bending motion is significantly higher ($\nu_2=1380\pm 20$ vs $606\ cm^{-1}$ for CH_3^+ and CH_3).[21–23]

Reactions of CH_3^+ with neutral molecules may proceed via reactive intermediates,[16,24] in which the ionic reactant and the neutral substrate are stabilized in a Lewis acid–base pair. Thermochemical measurements and *ab initio* calculations indicate that CH_3^+ acts as an efficient Lewis acid even with respect to the inert Ar atom.[13] The strong electrophilic character of CH_3^+ arises from the empty $2p_z$ orbital located on the central carbon atom. Due to participation of charge transfer in the binding mechanism, the intermolecular C–Ar bond in the CH_3^+-Ar complex is as strong as 47 ± 8 kJ/mol.[13] Because the CO molecule is a much better electron donor than Ar, the interaction in CH_3^+-CO (330 kJ/mol) is comparable to covalent bonds.[14] The interaction is maximized when the $2p_z$ orbital of CH_3^+ is directed towards the ligand. Therefore, complexes of the type CH_3^+-X, where X is an atom or diatom (e.g., Ar or CO), are characterized by a C_{3v} equilibrium structure. As an important exception, the CH_5^+ ion cannot be properly described by the $CH_3^+-H_2$ notation, because its five protons rapidly undergo exchange tunneling.[25,26]

Spectroscopic properties of CH_3^+ bound to a Lewis base may be expected to be intermediate between those of the free methyl radical and the methyl cation because the formation of such bonds is accompanied by a certain amount of charge transfer.[13] In the present work, the infrared spectrum of the CH_3^+-Ar complex is examined to compare its properties with those of CH_3 and CH_3^+. It is hoped that the systematic investigation of ionic complexes composed of CH_3^+ and various ligands X (e.g., X=rare gase atoms or small closed shell molecules) will provide valuable data to establish trends in the energetic, structural, and spectroscopic properties of the charge-transfer bonds involving the $2p_z$ orbital of carbon.

Thermochemical and theoretical studies of the $CH_3^+-Ar_n$ and $CH_3^+-(CO)_n$ series suggested that the $2p_z$ orbital of

a)Author to whom correspondence should be addressed.

TABLE I. Experimental and theoretical vibrational frequencies (in cm^{-1}) of CH_3 and CH_3^+ compared to those of $CH_3^+-Ar_n$ ($n=1,2$). Theoretical frequencies are derived from the nonrigid invertor model (nr.i.) (Ref. 38) or the local mode-coupled Morse oscillators model (l.m.) (Ref. 33).

Mode	CH_3 expt[a]	CH_3^+ expt[b]	CH_3^+-Ar expt[c]	$CH_3^+-Ar_2$ expt[c]	CH_3 nr.i.[d]	CH_3^+ nr.i.[e]	CH_3 l.m.[f]	CH_3^+-Ar l.m.[c]	$CH_3^+-Ar_2$ l.m.[c]
ν_1	3004.436(12)			2981(3)	3007.6	2900.7	3005	2979	2986
ν_2	606.4531(6)	1380(20)			609.3	1391.2			
ν_3	3160.82118(6)	3108.3770(57)	3145(30)	3151.6(5)	3160.9	3108.4	3171	3132	3148
ν_4	1396(1)[g]				1395.3	1399.0			
$2\nu_1$	5959.7(2.1)		5911.936(11)		5943.6	5664.6	5964	5915	5932
$\nu_1+\nu_3$			6027.70(17)[h]	6054(1)	6122.9	5859.1	6078	6020	6048
$2\nu_3$ ($l=0$)			6191.058(11)	6224(4)	6299.6	6083.4	6277	6204	6238
$2\nu_3$ ($l=2$)			6242.566(15)[h]	6284(2)	6307.5	6138.3	6318	6241	6274

[a]References 34, 58–61.
[b]References 20, 22.
[c]This work.
[d]References 35, 41.
[e]References 40, 41.
[f]Reference 33.
[g]Measured in a Ne matrix.
[h]Neglecting effects of ξ_3.

CH_3^+ can accept electron density from two ligands located at opposite sides of the CH_3^+ moiety.[13,14] However, while the C–C bonds in the $CH_3^+-(CO)_2$ complex (C_{3v} symmetry) were shown to be nonequivalent,[14] the equilibrium geometry of CH_3-Ar_2 was predicted to be of D_{3h} symmetry.[13] Further ligands ($n>2$) were supposed to occupy less symmetrical sites outside the C_3 axis on the basis of their lower incremental binding energies.[13] To test the conclusions derived from thermochemical and theoretical considerations, the spectroscopy of CH_3^+ surrounded by more than one Ar atom has also been investigated. Following the predictions based on thermochemical data only the first two ligands, attached to the $2p_z$ orbital of the carbon on both sides of the CH_3^+ plane, are expected to sensitively influence the spectroscopic properties of the ionic core. Subsequent Ar atoms, bound to the cluster by weaker inductive and van der Waals forces,[13] should have only a secondary effect on the vibrational frequencies. Significantly, the ν_3 spectrum of $CH_3^+-Ar_2$ obtained in the present work is rotationally resolved, providing the first example of extracting quantitative structural and dynamic information from a spectrum of a trimeric ionic complex. The structure of $CH_3^+-Ar_2$ is unambiguously shown to be of C_{3v} symmetry with two nonequivalent C–Ar bonds, in disagreement with previous predictions.[13] Results for the larger clusters are generally consistent with the assessments of the recent thermochemical study of the $CH_3^+-Ar_n$ series.[13]

Infrared spectra of $CH_3^+-Ar_n$ clusters have been recorded by means of photodissociation spectroscopy.[27] The power of this technique has previously been illustrated by the observation of infrared spectra of weakly bound ionic complexes such as $He-NH_4^+$ and $He-HCO^+$.[28,29] The present study of CH_3^+-Ar further demonstrates the high sensitivity and selectivity of this method by the detection of overtone vibrations of the CH_3^+ core at the level of rotational resolution. Other relevant Ar containing ionic complexes examined with a similar approach include $CH_5^+-Ar_n$ ($n=1,2$),[30] $NH_4^+-Ar_n$ ($n=1-7$),[31] and HCO^+-Ar_n ($n=1-13$).[32]

The interpretation of the observed spectra of $CH_3^+-Ar_n$ was greatly facilitated by the comparison with known spectroscopic properties of CH_3^+ and CH_3. All four fundamentals of CH_3 ($\nu_1-\nu_4$, Table I) and several overtone and combination bands [$2\nu_1$, $3\nu_1$, $n\nu_2(n\leqslant 4)$, and $\nu_1+2\nu_2$] have been characterized by Raman[33,34] and infrared absorption spectroscopy.[35] Based on the available spectroscopic data a stretching vibrational potential was constructed for CH_3 using the local mode-coupled Morse oscillator model, which could reproduce the frequencies of the CH stretching vibrations of CH_3 and its deuterated isotopomers to within a few wave numbers.[33] A slightly different selection of vibrational states was used[35–37] to determine the potential energy function of CH_3 based on the nonrigid invertor model.[38] These studies closely reproduced the available experimental data and also predicted frequencies of unknown transitions. The CH_3^+ ion has not been studied as extensively as CH_3 (Table I). An approximate value of its out-of-plane bending frequency was determined from photoelectron spectra as $\nu_2=1380(20)\ cm^{-1}$.[21,22] The degenerate ν_3 asymmetric stretching vibration was observed at $3108\ cm^{-1}$ by direct absorption spectroscopy.[20,39] The positions of other fundamental and overtone vibrations of CH_3^+ were predicted from an empirically corrected *ab initio* potential energy surface (Table I).[40,41]

Nearly all spectral features observed in the IR spectra of the $CH_3^+-Ar_n$ clusters can be correlated to intramolecular vibrations of the free CH_3^+ monomer. Hence, the notation employed for the cluster vibrations always refers to the four normal modes ($\nu_1-\nu_4$) of the CH_3^+ chromophore. The intermolecular stretch and bend vibrations of the CH_3^+-Ar dimer are designated ν_s and ν_b, respectively.

II. EXPERIMENT

The experimental setup and spectroscopic technique have been described in detail elsewhere.[42,43] Therefore, only the aspects relevant for the study of the $CH_3^+-Ar_n$ clusters are briefly summarized. Infrared photodissociation spectra were obtained by resonant excitation of mass-selected $CH_3^+-Ar_n$ clusters ($n=1-8$) into predissociating vibrational levels and monitoring the $CH_3^+-Ar_m$ ($m<n$) fragment ion current as a function of the excitation frequency. The experiments were carried out in a tandem mass spectrometer comprising an ion source, a first quadrupole mass filter for se-

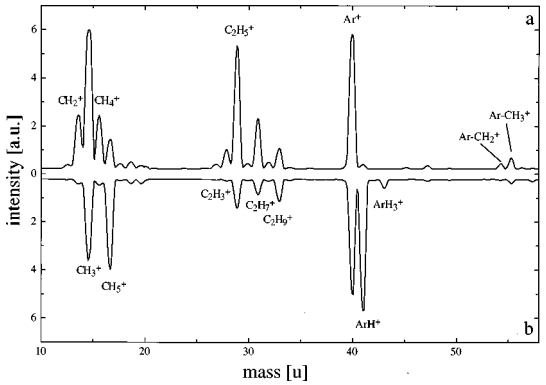

FIG. 1. Mass spectra obtained with the mixtures CH_4:He:Ar=1:100:500 (a) and CH_4:H_2:He:Ar=1:25:100:500 (b) at 5 bar stagnation pressure. Due to saturation effects, relative intensities can be compared only for peaks with intensities of less than 5 a.u. The spectra are dominated by ions of the form CH_n^+, $C_2H_n^+$ [and/or $C_2H_n^+-(H_2)_m$ and/or $CH_n^+-CH_4$], ArH_n^+ and CH_n^+-Ar. Though the addition of H_2 increases the relative abundance of CH_3^+ vs other CH_n^+ ions, it does not enhance the absolute ion currents of either CH_3^+ or CH_3^+-Ar.

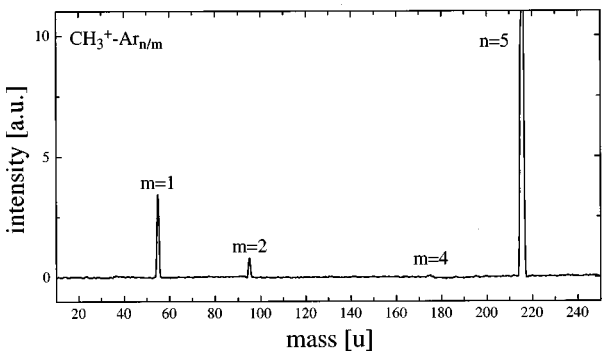

FIG. 2. Mass spectrum observed after excitation of the ν_3 vibration of mass selected $CH_3^+-Ar_5$ complexes. Fragment ions $CH_3^+-Ar_m$ with $m=1$, 2 are produced by laser action, while the signal at $m=4$ originates from metastable decay.

lecting the parent complex, an octopole ion guide where the cluster ions interact with the IR radiation and eventually dissociate, a second quadrupole mass spectrometer for selecting the fragment ions of interest, and an ion detector.

Cluster ions were produced in a pulsed (40 Hz) and skimmed electron impact supersonic expansion ion source. The optimum gas mixture for the production of $CH_3^+-Ar_n$ complexes contained CH_4, He, and Ar in a ratio of approximately 1:100:500 at 5–8 bar stagnation pressure [Fig. 1(a)]. The cluster distribution could be shifted to larger n by increasing the Ar concentration and the stagnation pressure. In agreement with previous studies,[20] addition of H_2 enhanced the relative production of CH_3^+ and CH_5^+ with respect to other CH_n^+ ions [Fig. 1(b)]. However, the absolute ion currents of $CH_3^+-Ar_n$ complexes were not improved as H_2 competed with Ar in the clustering reactions. Furthermore, the CH_4 concentration had to be kept below 1% in order to avoid extensive polymerization reactions leading to larger $C_2H_n^+$ ions.

Due to the high binding energy of CH_3^+-Ar ($\approx 4000\ cm^{-1}$),[13] the photodissociation signal of $CH_3^+-Ar_n$ complexes with $n \leqslant 2$ appeared in the $m=n-1$ fragment ion channel where it interfered with the signal arising from metastable decay of internally hot complexes in the octopole. In order to separate these two contributions the nozzle of the ion source was triggered at twice the laser frequency, and the laser-off signal was subtracted from the laser-on signal. Larger clusters ($n \geqslant 3$) could shed more than one Ar atom following absorption, as the photon energy substantially exceeded the binding energy of the Ar ligands with $n>2$ ($\approx 700\ cm^{-1}$).[13] Therefore, only little interference with the metastable decay signal was observed, which mainly occurred in the $m=n-1$ fragment channel. For a given parent cluster size, the observed range of fragment channels arising from laser induced dissociation was rather small. For example, the mass spectrum measured with the second quadrupole mass spectrometer after photoexcitation of mass selected $CH_3^+-Ar_5$ complexes (Fig. 2) exhibits $CH_3^+-Ar_m$ fragment peaks with $m=1$ and 2 arising from laser action, while the small peak at $m=4$ originates from metastable decomposition. As the spectra recorded in different fragment channels were observed to be very similar, only one is presented in the respective figures.

Tunable IR radiation was generated by a Nd:YAG laser pumped optoparametric oscillator (OPO) system characterized by $0.02\ cm^{-1}$ bandwidth, 5 ns pulse duration, 20 Hz repetition rate, a tuning range of $2500-6900\ cm^{-1}$ and an intensity of 0.5–5 mJ/pulse depending on the wavelength. The laser power measured with an InSb photovoltaic detector was used to normalize the photofragmentation signal assuming a linear power dependence. The recorded spectra were calibrated against known infrared absorptions of NH_3 and HDO using the signal and idler outputs of the OPO laser.[44] A small Doppler correction was added to the measured wave numbers to compensate for the kinetic energy (several eV) of the ions in the octopole. The uncertainty in the ion kinetic energy and the laser bandwidth limited the absolute precision of line positions to $0.01\ cm^{-1}$.

Spectra of $CH_3^+-Ar_n$ clusters with $n=2-8$ were recorded between 3100 and $3200\ cm^{-1}$ which corresponds to the region of the strong infrared active asymmetric CH stretching fundamental of CH_3^+ (ν_3). Because of its high binding energy ($3950 \pm 700\ cm^{-1}$),[13] the CH_3^+-Ar dimer does not predissociate from the ν_3 and ν_1 (symmetric CH stretch) vibrational states. Consequently, only hot band transitions terminating at levels above the lowest dissociation

TABLE II. Calculated CH bond length (r) and scaled harmonic frequencies of CH_3^+ (D_{3h}) compared to available experimental values. IR intensities (in km/mol) are given in brackets.

Level	r (Å)	ν_1 (a_1') (cm^{-1})	ν_2 (a_2'') (cm^{-1})	ν_3 (e') (cm^{-1})	ν_4 (e') (cm^{-1})
HF/B	1.0797	2924 (0)	1387 (5)	3108 (130)	1400 (33)
MP2/6-311G[a]	1.089				
MP2/A	1.0845	2912 (0)	1357 (7)	3108 (140)	1377 (31)
MP2/B	1.0844				
expt	~ 1.087[b]		1380 ± 20[c]	3108.4[b]	

[a]Reference 13.
[b]Reference 20.
[c]Reference 22.

TABLE III. Structure, scaled harmonic frequencies, and energetics of the global minimum structure (C_{3v}) of CH_3^+–Ar. IR intensities (in km/mol) are given in brackets.

Level	r (Å)	R (Å)	θ	E_1 (cm^{-1})	E_2 (cm^{-1})	D_e (cm^{-1})	ν_1 (a_1) (cm^{-1})	ν_2 (a_2) (cm^{-1})	ν_3 (e) (cm^{-1})	ν_4 (e) (cm^{-1})	ν_s (a_1) (cm^{-1})	ν_b (e) (cm^{-1})
HF/B	1.0754	2.3617	93.2	2332.7	309.6	2023.1	2959 (5)	1338 (12)	3145 (103)	1406 (28)	157 (134)	632 (1)
MP2/6-311G[a]	1.086	2.374	93.8			3740[b]						
MP2/A	1.0786	1.9884	99.0	7781.6	2206.0	5575.6	2961 (6)	1331 (19)	3136 (74)	1395 (29)	370 (147)	945 (0)
MP2/B	1.0795	1.9543	99.6	8912.3	2501.2	6411.1						

[a]Reference 13.
[b]Single point calculation at the MP4/6-311G* level ($D_0 = 3290\ cm^{-1}$).

threshold can be detected in the 3 μm range by the present experimental approach (e.g., $2\nu_3 \leftarrow \nu_3$). However, excitation of two quanta of the CH stretch vibrations of CH_3^+ is sufficient to induce dissociation of the dimer, and therefore the range between 5700 and 6700 cm^{-1} was also examined in order to locate the overtone and combination bands $2\nu_3$, $2\nu_1$, and $\nu_1+\nu_3$ of CH_3^+–Ar and CH_3^+–Ar_2.

III. *AB INITIO* CALCULATIONS

To guide the interpretation of the experimental results, *ab initio* calculations have been performed using the GAUSSIAN 94 program package.[45] The basis set used for the monomer and dimer consisted of an Ahlrichs VTZ basis augmented with diffuse and polarization functions taken from the aug-cc-pVTZ basis set (basis B).[46] The contraction scheme can be described as $H(6s3p2d) \rightarrow [4s3p2d]$, $C(11s7p3d2f) \rightarrow [7s4p3d2f]$, and $Ar(13s10p3d2f) \rightarrow [8s6p3d2f]$. For the larger complexes ($n \geqslant 2$), the basis was reduced by removing the d functions on H and the f functions on C and Ar (basis A). All coordinates were allowed to relax during the search for stationary points. For the evaluation of intermolecular well depths (D_e) the energies obtained from the geometry optimization were first corrected for basis set superposition error using the counterpoise method of Boys and Bernardi.[47] The energies derived in this manner (E_1) were further corrected for the relaxation energies (E_2) that arise from the changes in the geometry of the monomer(s) upon complexation.[48] The results of the calculations are summarized in Tables II–V and Figs. 3 and 4. Evaluated harmonic frequencies at the HF (MP2) level were scaled with the factor 0.919 (0.942) to match the experimental value for the ν_3 frequency of CH_3^+. The tables also include available experimental data and results of a previous *ab initio* calculation on CH_3^+–Ar_n complexes ($n=0-3$) (Ref. 13) at the MP2/6-311G level of theory.

The calculations for the CH_3^+ monomer were conducted to investigate the changes of its properties induced by the complexation with Ar ligands. As expected, geometry optimizations resulted at all levels of theory in a D_{3h} equilibrium structure [Fig. 3(a) and Table II] with a CH bond length in reasonable agreement with the experimental value.[20] The scaled harmonic frequencies (other than ν_3) were also close to those derived from experiments and the nonrigid inverter model (Tables I and II).

The global minimum found on the CH_3^+–Ar intermolecular potential energy surface corresponds to a C_{3v} (''π-bound'') configuration, whereby the Ar atom is attached to the empty $2p_z$ orbital of CH_3^+ [Fig. 3(b) and Table III]. The Ar atom donates electron density into this strongly electrophilic orbital which significantly distorts the CH_3^+ moiety. It appears that complexation with Ar transforms the sp^2 hybridization in the planar CH_3^+ monomer towards the sp^3 case leading to a pyramidal-like structure of CH_3^+–Ar.

At the HF level of theory (HF/B) the CH bond is shortened by 0.004 Å upon complexation with the first Ar atom, while the angle θ increases from 90° to 93°. The energy for this CH_3^+ deformation amounts to $E_2 = 310\ cm^{-1}$. According to the Mulliken analysis, the formation of the intermolecular bond ($D_e = 2023\ cm^{-1}$, $R = 2.36$ Å) is accompanied by a charge transfer of $\Delta Q \approx 0.15e$ from Ar to C. The inclusion of

TABLE IV. Calculated structural and energetic properties of isomeric structures of the CH_3^+–Ar dimer [Figs. 3(b)–3(d)].

Structure	Level	$r(r_1/r_2)$ (Å)	R (Å)	θ/φ	E_1 (cm^{-1})	E_2 (cm^{-1})	D_e (cm^{-1})
π-bound (C_{3v})	MP2/B	1.0795	1.9543	99.6	8912.3	2501.2	6411.1
Vertex-bound (C_{2v})	MP2/B	1.0868/1.0845	3.5147	119.6	679.7	1.5	678.2
	MP2/6-311G[a]	1.090/1.090	4.000	119.9			385
Side-bound[b] (C_{2v})	MP2/B	1.0843/1.0843	3.4096	119.4	595.8	1.7	594.1

[a]Reference 13.
[b]Transition state.

TABLE V. Comparison of calculated geometries, frequencies, and binding energies of CH_3^+–Ar_n complexes ($n=0-2$, Fig. 3). IR intensities (in km/mol) are given in brackets.

n	Symmetry	Level/basis	r (Å)	$R(R_1/R_2)$ (Å)	θ	D_e (cm^{-1})	ν_1 (cm^{-1})	ν_2 (cm^{-1})	ν_3 (cm^{-1})	ν_4 (cm^{-1})
0	D_{3h}	MP2/A	1.0845				2912 (0)	1357 (7)	3108 (140)	1377 (31)
1	C_{3v}	MP2/A	1.0786	1.9884	99.0	5575.6	2961 (6)	1331 (19)	3136 (74)	1395 (29)
2	C_{3v}	MP2/A	1.0778	2.0424/2.8776	97.5	767.6	2964 (2)	1303 (36)	3149 (77)	1389 (22)
	D_{3h}	MP2/A[a]	1.0771	2.3692	90.0	221.9	2965 (0)	1269 (75)	3168 (94)	1380 (19)
	D_{3h}[b]	MP2/6-311G	1.085	2.620	90.0	980				

[a]Transition state.
[b]Reference 13.

electron correlation (MP2/B) causes the intermolecular bond to become drastically stronger and shorter ($D_e=6411\ cm^{-1}$, $R=1.95$ Å). Consequently, the CH_3^+ geometry is more affected by complexation. The CH bond shrinks by around 0.005 Å, while the angle θ increases to nearly 100°. The stronger monomer distortion is reflected in a larger relaxation energy of $E_2=2501\ cm^{-1}$. The amount of transferred charge increases as well ($\Delta Q\approx 0.3e$). To investigate the influence of the Ar atom on the CH_3^+ monomer, several properties of the dimer were calculated at various intermolecular separations R of the Ar atom along the C_3 axis of CH_3^+. Figure 4 illustrates the dependence of the structural parameters (r and θ), the transferred charge (ΔQ) and the energies (E_2 and D_e) on R.

It appears that the lack of polarization functions in the previous MP2/6-311G calculation[13] led to an underestimation of the intermolecular bond strength in the CH_3^+–Ar dimer. The results of that study ($R=2.374$ Å, $\theta=94°$, $\Delta Q=0.17e$, $D_e=3740\ cm^{-1}$) are close to those obtained in the present work at the HF level using somewhat larger basis sets (Table III). In contrast, at the MP2/B level ($D_e=6411\ cm^{-1}$) the intermolecular bond strength is somewhat overestimated, while it is well reproduced at the MP2/A level ($D_e=5576\ cm^{-1}$). Estimation of the zero-point energy correction by considering only the intermolecular frequencies gives $D_0\approx 4450\ cm^{-1}$ at the MP2/A level, which falls within the error limits of the experimental value ($-\Delta H_0=3950\pm 700\ cm^{-1}$).[13]

Two further structures of the dimer potential energy surface have been investigated (Table IV, Fig. 3). The planar vertex-bound C_{2v} structure [Fig. 3(c)] turned out to be a local minimum, whereas the side-bound planar C_{2v} geometry [Fig. 3(d)] represents a transition state. Both structures possess significantly weaker and longer intermolecular bonds ($D_e=678$ and $594\ cm^{-1}$) compared to the global minimum configuration ($D_e=6411\ cm^{-1}$, MP2/B). Consequently, the CH_3^+ monomer is nearly unaffected by complexation, which is also reflected in the negligible monomer distortion energies ($E_2<2\ cm^{-1}$). As almost no charge is transferred from Ar to the CH_3^+ moiety ($\Delta Q<0.02e$), induction interactions dominate the attractive part of the intermolecular potential for these two planar hydrogen-bonded structures. The properties obtained for the vertex-bound local minimum agree only qualitatively with those reported previously (MP2/6-311G),[13] as the inclusion of polarization functions in the present work increases the bond strength by nearly a factor 2 (Table IV).

The barrier for internal rotation of the CH_3^+ unit within the CH_3^+–Ar dimer can be roughly estimated as $\approx 6000\ cm^{-1}$ (MP2/B) from the difference of the energies of the π-bound global minimum and those of the side-bound and vertex-bound structures. As this barrier is much larger than the rotational constant of CH_3^+ ($B\approx 9.4\ cm^{-1}$),[20] the internal rotation is completely quenched. The large angular anisotropy of the CH_3^+–Ar intermolecular potential is also

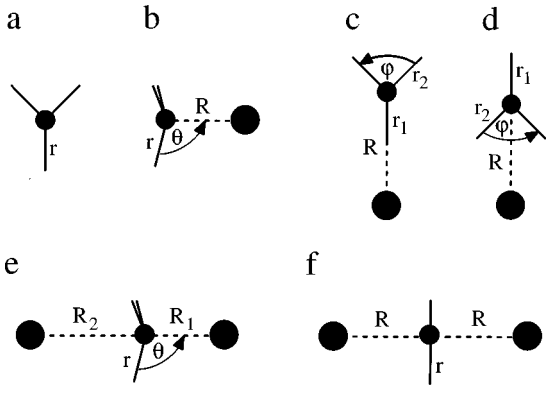

FIG. 3. Structures of CH_3^+–Ar_n complexes ($n=0-2$): (a) $n=0$ (D_{3h}); (b) $n=1$, π-bound global minimum (C_{3v}); (c) $n=1$, vertex-bound local minimum (C_{2v}); (d) $n=1$, side-bound transition state (C_{2v}); (e) $n=2$, global minimum (C_{3v}); (f) $n=2$, transition state (D_{3h}).

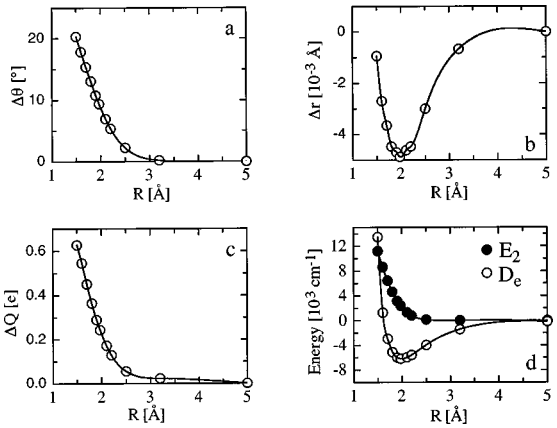

FIG. 4. Various properties of CH_3^+–Ar (C_{3v}) as a function of the intermolecular separation R (evaluated at the MP2/B level): (a) $\Delta\theta=\theta-90°$; (b) $\Delta r=r_{complex}-r_{monomer}$; (c) transferred charge ΔQ; (d) energies E_2 and D_e.

mirrored in the high harmonic, intermolecular bending frequency of the π-bound C_{3v} structure ($\nu_b = 945\ \mathrm{cm}^{-1}$, MP2/A), which is substantially larger than the corresponding intermolecular stretching frequency ($\nu_s = 370\ \mathrm{cm}^{-1}$).

The previous calculation predicted the symmetric D_{3h} structure with two equivalent Ar atoms as the global minimum of the CH_3^+–Ar_2 trimer surface [Fig. 3(f)].[13] The intermolecular separation increased from 2.374 to 2.620 Å upon the attachment of the second Ar atom, resulting in a significant drop in the incremental dissociation energy (D_e) from 3740 cm^{-1} for $n=1$ to 980 cm^{-1} for $n=2$.[13] In the present study the symmetric D_{3h} structure is also calculated to be the global minimum at the HF/B level. However, at the MP2/A level this structure becomes a transition state ($D_e = 222\ \mathrm{cm}^{-1}$) between two equivalent C_{3v} global minima [$D_e = 768\ \mathrm{cm}^{-1}$, Fig. 3(e)]. The latter contain two nonequivalent Ar atoms with substantially differing intermolecular separations ($R_1 = 2.04$ Å, $R_2 = 2.88$ Å). The configuration can be described as a pyramidal CH_3^+–Ar dimer core that is only little perturbed by the second Ar atom. The slight destabilization (lengthening) of the intermolecular bond to the first Ar atom is accompanied by a small decrease in r, θ, and the transferred charge. These observations are in line with the trends shown in Fig. 4 for increasing R in the CH_3^+–Ar dimer. The second Ar atom donates only little charge to the CH_3^+ ion, implying that this weak bond mainly arises from inductive interactions.

The calculated intermolecular bond lengths for the symmetric transition state (D_{3h}) are $R = 2.37$ Å, i.e., intermediate between those of the global minimum (C_{3v}). According to the Mulliken analysis, there is only little charge transferred from the two Ar atoms to the central ion, indicating that both bonds are governed by polarization forces. The difference between the energies of the global minimum and the transition state corresponds to the barrier height (V_b) for the umbrella-type tunneling motion of the complex, which amounts to 550 cm^{-1} at the MP2/A level of theory.

Apparently, the nature of the stationary point with D_{3h} symmetry on the trimer potential energy surface sensitively depends on the computational level. Calculations conducted at the HF/A and MP2/6-311G (Ref. 13) levels predict the D_{3h} structure to be the global minimum. However, both approaches underestimate the strength of the intermolecular bond to the first Ar atom due to the neglect of electron correlation in the first case and the lack of polarization functions for the geometry optimizations in the second case. On the other hand, the structural and energetic properties of CH_3^+–Ar_n ($n=0-2$) obtained at the MP2/A level are consistent with the experimental results discussed below. In particular, splittings in the spectra of the $n=2$ complex attributed to the inversion motion of the CH_3^+ core within the CH_3^+–Ar_2 trimer confirm that the C_{3v} geometry is indeed the global minimum. Furthermore, the intermolecular well depths (D_e) for CH_3^+–Ar and CH_3^+–Ar_2 of 5580 and 770 cm^{-1} calculated at the MP2/A level are consistent with the measured bond enthalpies of 3950 ± 700 and $790 \pm 70\ \mathrm{cm}^{-1}$,[13] adding some evidence that the level of theory employed in the present work may be sufficient for a reliable description of the intermolecular bonds in CH_3^+–Ar and CH_3^+–Ar_2.

IV. EXPERIMENTAL RESULTS AND DISCUSSION

A. CH_3^+–Ar dimer

Figure 5 reproduces the recorded photofragmentation spectrum of the CH_3^+–Ar dimer. A weak, unresolved and broad feature (FWHM$\approx$130 cm^{-1}) is observed at 3145 cm^{-1}, i.e., close to the strong transition of the asymmetric stretching vibration of the monomer ($\nu_3 = 3108.4\ \mathrm{cm}^{-1}$). However, the ν_3 frequency of the complex is well below its lowest dissociation threshold ($\approx 4\times10^3\ \mathrm{cm}^{-1}$) and therefore the ν_3 fundamental cannot appear in a one-photon photodissociation spectrum. Consequently, the broad feature is attributed to overlapping sequence transitions of the type $\nu_x + \nu_3 \leftarrow \nu_x$ where ν_x represents a vibration with a frequency in excess of $\approx 10^3\ \mathrm{cm}^{-1}$. The symmetric stretching mode (ν_1) has a slightly lower frequency than ν_3 ($2900 < \nu_1 < 3000\ \mathrm{cm}^{-1}$, Tables I–III) and is dipole forbidden for the monomer. However, due to symmetry reduction it becomes weakly allowed in the complex. Therefore, the red wing of the broad feature ($\leqslant 3000\ \mathrm{cm}^{-1}$) may also contain sequence transitions of the form $\nu_x + \nu_1 \leftarrow \nu_x$. The presence of hot bands is a characteristic feature of the spectra of other ionic complexes produced under similar experimental conditions in this ion source. A further contribution to the photodissociation signal in this frequency range may arise from resonant two-photon absorption via the ν_3 (or ν_1) intermediate state. Neglecting the effects of cross anharmonicities, the ν_3 frequency of the CH_3^+–Ar complex can be estimated from the weighted average position of the observed broad feature as $3145 \pm 30\ \mathrm{cm}^{-1}$, in good agreement with the scaled *ab initio* frequencies (Table III). This value is closer to the ν_3 frequency of the CH_3 radical (3160.8 cm^{-1}) (Ref. 49) than to that of the CH_3^+ ion (3108.4 cm^{-1}).[20]

As the frequencies of the first CH stretching overtones exceed the dissociation threshold of the complex, they can be seen in the photodissociation spectrum as transitions originating from the vibrational ground state. Five rotationally resolved bands appear between 5700 and 6700 cm^{-1} (Fig. 5, Table VI). The widths of single rotational lines are limited by the laser bandwidth (0.02 cm^{-1}) indicating upper state lifetimes of at least 250 ps. Two transitions, with origins at 6191 and 5912 cm^{-1}, exhibit the structure expected for a parallel transition in a prolate symmetric top molecule. The other three bands are perpendicular transitions, with band centers at 6243, 6028, and 5870 cm^{-1} and strong unresolved Q branch heads of the respective $\Delta K = \pm 1$ subbands. For the strongest subbands, series of P and R branch lines ($\Delta J = \pm 1$) could be identified as well.

The vibrational assignment of the observed bands is based on their structure, position, and relative intensity, and available experimental and theoretical data for the CH_3^+ and CH_3 monomers. As the Ar atom is attached to the $2p_z$ orbital of the CH_3^+ moiety its influence on the in-plane vibrational frequencies of the core ion (ν_1, ν_3, and ν_4) is small. Three overtone and combination bands of the CH stretch vibrations, namely $2\nu_3$, $\nu_1+\nu_3$, and $2\nu_1$, are anticipated in the

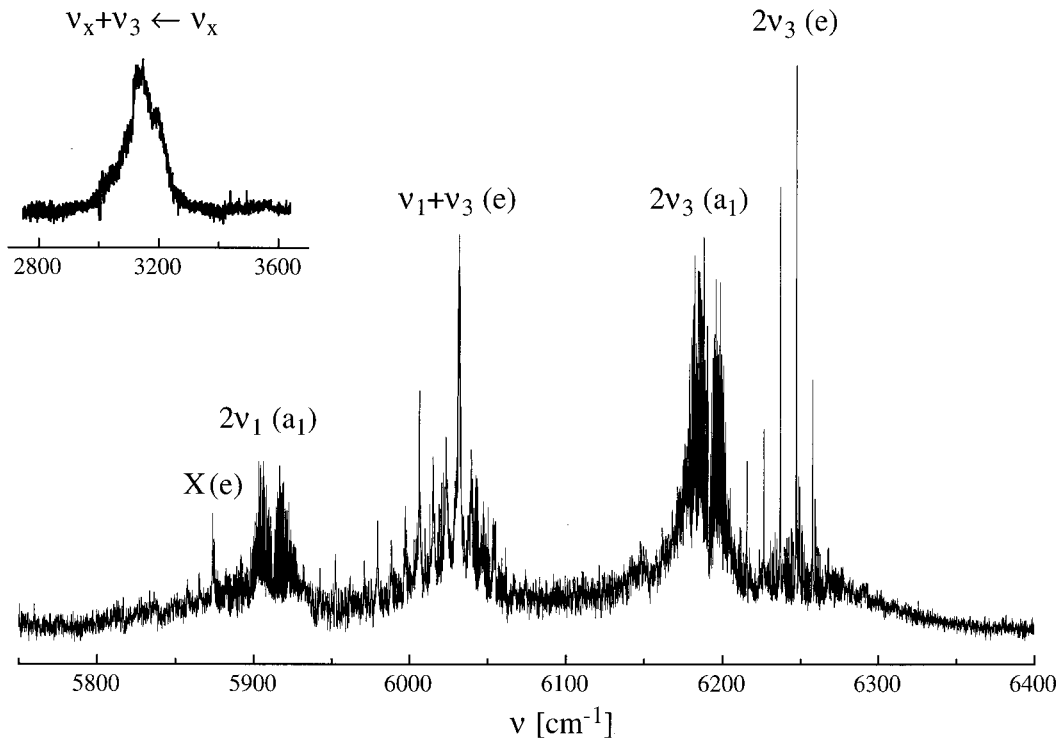

FIG. 5. Overview of the photodissociation spectrum of CH_3^+–Ar in the region of the first CH stretch overtones. The inset shows the spectrum in the ν_3 frequency range.

studied spectral range with intensities and transition frequencies dropping in the above-mentioned order. The four stronger bands in the CH stretch overtone range of the CH_3^+–Ar spectrum are assigned as indicated in Fig. 5 and Table VI. The parallel band at 6191 cm^{-1} and the perpendicular band at 6243 cm^{-1} (Fig. 6) are attributed to the transitions into the a_1 ($l=0$) and e ($l=2$) components of the first ν_3 overtone. These two bands occur at roughly twice the frequency of the unresolved feature at 3145(30) cm^{-1} associated with sequence bands involving ν_3. The observed red shift arises from anharmonic effects. The splitting between the a_1 and e subcomponents of $2\nu_3$ ($\approx 52\ cm^{-1}$) would correspond to $4g_{33}$ if the off-diagonal interactions between $2\nu_1(a_1)$ and $2\nu_3(a_1)$ and between $\nu_1+\nu_3(e)$ and $2\nu_3(e)$ were neglected.[50] The perpendicular band at 6028 cm^{-1} is assigned as $\nu_1+\nu_3(e)$ combination band ($l=1$), while the parallel band at 5912 cm^{-1} is interpreted as $2\nu_1(a_1)$ overtone (Fig. 7). Whenever the construction of lower state combination differences was possible, they confirmed that the rotationally resolved bands originate from the same vibrational level, the ground state of the complex. The weak perpendicular transition (denoted X) with origin at 5870 cm^{-1} has not been assigned yet.

The proposed vibrational assignment is compatible with the expectation that the partial charge transfer from the Ar atom to the CH_3^+ core should shift the CH stretching frequencies towards those of the neutral CH_3 radical. Table I compares the vibrational origins of the assigned bands in the photodissociation spectrum of CH_3^+–Ar with known or predicted vibrational frequencies of the methyl radical and its

TABLE VI. Spectroscopic constants of vibrational states of CH_3^+–Ar obtained from the fit of experimental line positions[a] to the Hamiltonian given in Eq. (1). Values in brackets correspond to 2σ confidence limits.

Vibrational state	Molecular constant	Value (cm^{-1})
ground state (a_1)	B	0.35275(32)
	D_J ($\times 10^6$)	2.14(65)
	D_{JK} ($\times 10^4$)	1.00(37)
	D_K ($\times 10^4$)	2.6(7.6)
$2\nu_3$ (a_1)	ν_0	6191.058(11)
	ΔA	−0.0777(26)
	B	0.35302(34)
	D_J ($\times 10^6$)	2.62(70)
	D_{JK} ($\times 10^4$)	1.39(41)
	D_K ($\times 10^4$)	2.5(7.7)
$2\nu_3$ (e)	$\nu_0-2A\xi$	6242.566(15)
	$A(1-2\xi)$	5.539(11)
	ΔA	−0.065(13)
	B	0.35202(52)
	D_J ($\times 10^6$)	6.0(3.1)
	D_{JK} ($\times 10^4$)	1.81(87)
	D_K ($\times 10^4$)	31(14)
$2\nu_1$ (a_1)	ν_0	5911.936(11)
	ΔA	−0.0853(48)
	B	0.35157(31)
	D_J ($\times 10^6$)	2.36(54)
	D_{JK} ($\times 10^4$)	0.92(38)
	D_K ($\times 10^4$)	13.4(8.6)
$\nu_1+\nu_3$ (e)	$\nu_0-A\xi$	6027.70(17)
	$A(1-\xi)-B$	3.966(22)
	$\Delta A-\Delta B$	−0.115(13)
X (e)	$\nu_0-Al\xi$	5870.2(3)
	$A(1-l\xi)-B$	4.06(5)

[a]Line positions are available upon request.

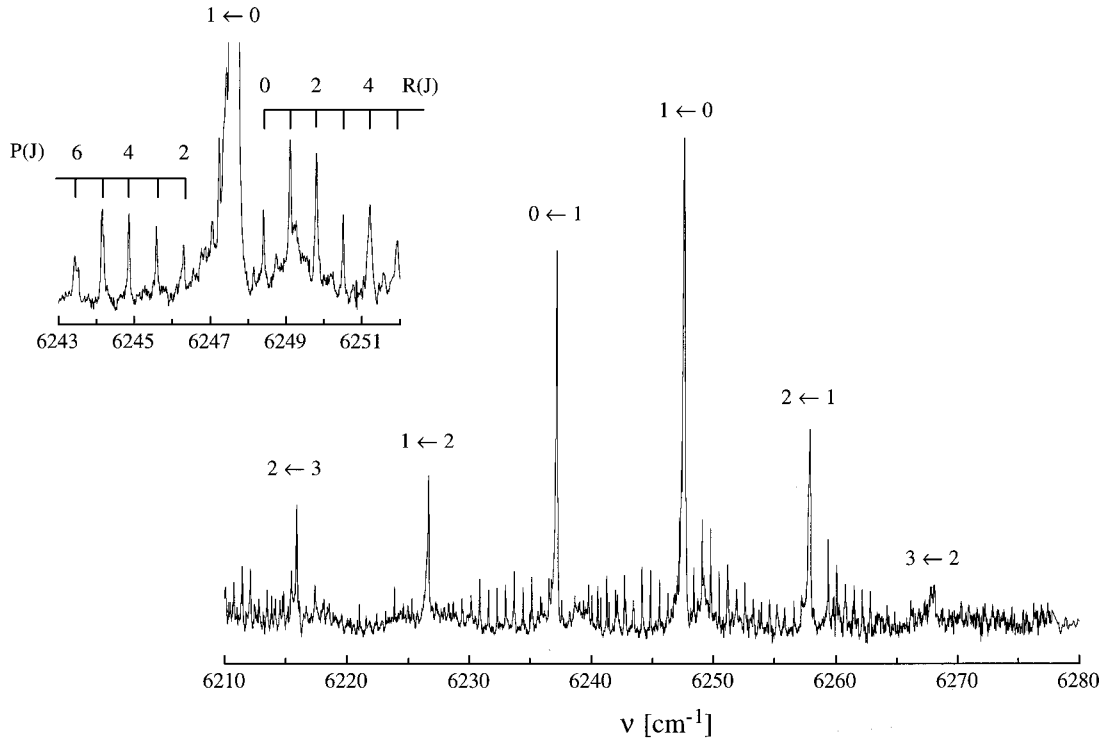

FIG. 6. Photodissociation spectrum of the $2\nu_3(e)$ band of CH_3^+–Ar with assignments of the $K_a' \leftarrow K_a''$ Q branches. The inset shows $1 \leftarrow 0$ subband in more detail, along with P and R branch line assignments.

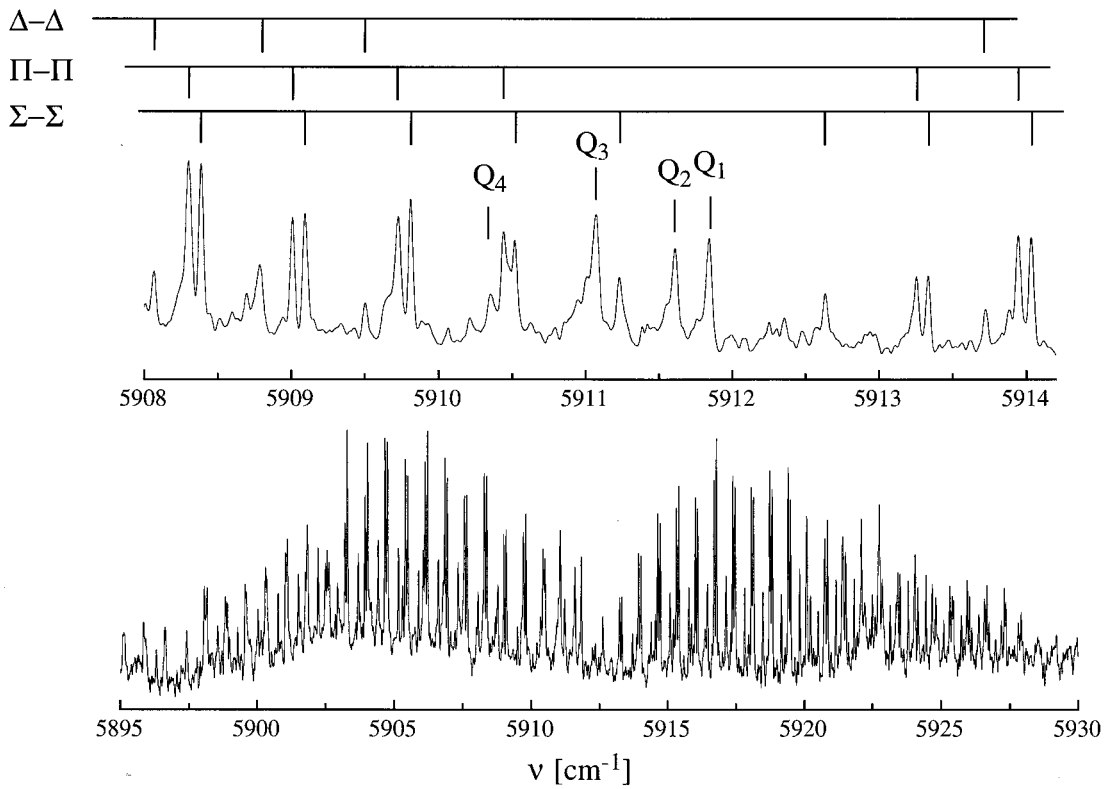

FIG. 7. Photodissociation spectrum of the $2\nu_1$ band of CH_3^+–Ar (bottom). The top trace shows the center of this parallel transition along with assignments of the unresolved Q branches and the P and R branch rotational lines of the $\Delta K_a = 0$ subbands.

cation. The vibrational energies of the CH_3^+–Ar complex are in all cases bracketed by the corresponding frequencies of CH_3^+ and CH_3. Moreover, they are much closer to the CH_3 values indicating that the amount of charge transferred from the Ar atom to the $2p_z$ orbital of CH_3^+ is substantial, in agreement with the *ab initio* calculations.

The positions of the CH stretching vibrational bands of CH_3^+–Ar can be described with reasonable accuracy by a local mode-coupled Morse oscillator model.[33] Only three parameters, a frequency (ω_m), an anharmonicity constant (χ_m) and an interbond coupling parameter (λ_m) are necessary to describe the fundamentals, overtones, and combination bands of identical local mode oscillators. The parameters obtained from a least squares fit of the complex's transitions [$\omega_m = 3183(28)$ cm^{-1}, $\chi_m = -51(3)$ cm^{-1}, $\lambda_m = -51(11)$ cm^{-1}] are similar to those of CH_3 and its deuterated isotopomers ($\omega_m = 3223$ cm^{-1}, $\chi_m = -55$ cm^{-1}, $\lambda_m = -54.2$ cm^{-1}).[33] The fit predicts the frequency of the ν_1 symmetric stretching vibration of CH_3^+–Ar as 2979 cm^{-1}, which is again closer to the respective CH_3 value (3004 cm^{-1}) than to the one predicted for CH_3^+ (2901 cm^{-1}). Moreover, it agrees well with the scaled *ab initio* frequencies of 2961 and 2959 cm^{-1} evaluated for CH_3^+–Ar at the HF/A and MP2/B levels.

The assignment of the rotational quantum numbers K and J in the observed transitions was based on several factors. For perpendicular transitions, the $K=1\leftarrow 0$ Q branch head is expected to be the strongest feature in the band (Fig. 6). The $K=0\leftarrow 0$ subband of parallel transitions can also be identified by its relative strength and the lack of a Q branch (Fig. 7). Other subbands of the parallel transitions have weak Q branches and their positions are linked together via a K^2 dependence. The assignment can be verified by the observation of missing rotational lines with $J<K$ in the P and R branches. However, this criterion is not always conclusive due the overlap of interfering lines. Finally, the K assignments were consistent with the nuclear spin statistics for a C_{3v} molecule with three equivalent protons, which gives rise to a twofold statistical weight for bands originating from $K=3n$ ($n>0$). This distinct intensity alternation could be seen in the recorded spectra.

The line positions of the rotationally resolved bands were least-squares fitted to a standard semirigid prolate symmetric top Hamiltonian taking into account first order Coriolis coupling,[50]

$$F(J,K) = \nu_0 + BJ(J+1) + (A-B)K^2 - D_J J^2 (J+1)^2 - D_{JK} J(J+1)K^2 - D_K K^4 - 2\xi lAK. \quad (1)$$

For vibrational states with a_1 symmetry the vibrational angular momentum l is zero. The transitions into the e and a_1 components of $2\nu_3$ (117 and 87 lines, respectively) were fitted together with the $2\nu_1$ band (132 lines) to obtain the molecular constants for the ground and the respective upper vibrational states. The molecular constants from this simultaneous fit (rms=0.025 cm^{-1}) are summarized in Table VI. With a few exceptions, they could reproduce all experimental lines of the $2\nu_1$, $2\nu_3$ (e), and $2\nu_3$ (a_1) bands to better than 0.02, 0.03, and 0.05 cm^{-1}, which is of the order of the laser resolution (0.02 cm^{-1}). The largest deviations are observed for partly overlapping lines and the few transitions involving high K values ($K\geqslant 3$) for which higher order terms neglected in the Hamiltonian (1) may be significant. For the fits of the perpendicular bands $\nu_1+\nu_3$ and X only Q branches (11 and 5 data points, respectively) were used to determine the respective molecular constants (Table VI).

The observed rovibrational transition frequencies do not allow for the independent determination of the molecular constants A'', A', ξ_3, and $\nu_0(e)$. Even if this were the case, isotopic substitution experiments would be required to deduce both the angle θ and the intramolecular C–H bond length r from the rotational constants. Therefore, the C–Ar separation R was estimated from the B constant (0.352 75 cm^{-1}) assuming that the CH_3^+ moiety adopts the structure predicted by the *ab initio* calculations ($\theta=99.0°$, $r=1.0786$ Å, MP2/A). The distance R calculated in this way amounts to 2.018 Å, which is in reasonable agreement with the *ab initio* value of $R_e=1.988$ Å (MP2/A). Treating the complex as a pseudodiatomic with an undistorted monomer structure yields a similar separation of $R=2.053(3)$ Å, and a harmonic intermolecular stretching force constant of 51(17) N/m with a corresponding frequency of 281(46) cm^{-1}. It is noted, that the *ab initio* structure for CH_3^+–Ar given in Ref. 13 gives a B constant (0.263 cm^{-1}) well below the experimental value due to a significant underestimation of the intermolecular interaction.

The intermolecular bond length in CH_3^+–Ar ($R\approx 2.0$ Å) is comparable to the Ar–H separation in the relatively strongly bound Ar–HN_2^+ ionic complex ($R\approx 1.9$ Å, $D_0\approx 2780$ cm^{-1}).[51] Though the binding energy of the CH_3^+–Ar complex is apparently higher, the larger size of the carbon atom does not permit a closer approach compared to the linear proton-bound Ar–HN_2^+ complex. A comparison with the geometry of CH_3Cl is also interesting as it is isoelectronic with CH_3^+–Ar, but has a fully developed covalent bond. The structural parameters of CH_3Cl are $r_{CH}=1.085$ Å, $r_{CCl}=1.776$ Å, and $\theta=108.6°$.[52] As expected, the stronger bond in methyl chloride ($D_0=3.57$ eV $\approx 28\,800$ cm^{-1}) (Ref. 53) leads to a shorter interatomic separation and a larger interbond angle, which is typical for an sp^3 hybridized carbon ($\theta=109.5°$ for CH_4).

The binding energy of CH_3^+–Ar may also be compared with those of the related CH_3^+–Kr and CH_3^+–Xe complexes. The observation of the first ν_1 overtone and the lack of the ν_3 fundamental in the CH_3^+–Ar photofragmentation spectrum allows to bracket the complex's binding energy between 3150 and 5900 cm^{-1}, in agreement with thermochemical measurements (11.3 ± 2 kcal/mol$\approx 3950\pm 700$ cm^{-1}) (Ref. 13) and the *ab initio* predictions (≈ 4450 cm^{-1}, MP2/A). The methyl cation binding energies of Kr and Xe have been measured as 47.7 ± 2.5 and 55.2 ± 2.5 kcal/mol, respectively.[24,54] The relatively large binding energies of CH_3^+–Kr and CH_3^+–Xe indicate that the bonds between CH_3^+ and the rare gas atoms Kr and Xe are dominated by covalent interactions rather than electrostatic forces.[54,55] For a large number of molecules a linear correlation between their proton and methyl cation affinities has

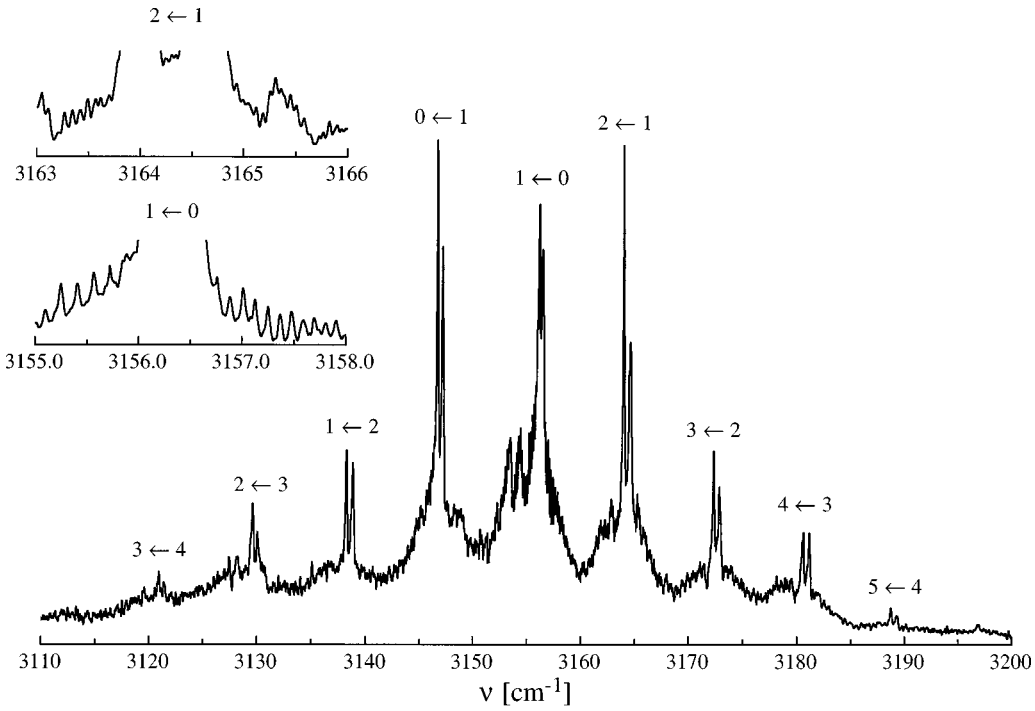

FIG. 8. Photodissociation spectrum of the ν_3 band of CH_3^+–Ar_2 with assignments of the $K_a' \leftarrow K_a''$ Q branches. The inset shows the structure of the $1 \leftarrow 0$ and $2 \leftarrow 1$ subbands in more detail.

been found. However, in contrast to the rare gas atoms Kr and Xe, this relation does not hold for Ar, as it predicts for CH_3^+–Ar a binding energy of 44 kcal/mol (Ref. 54) which substantially deviates from the above-mentioned experimental and *ab initio* values. The fact that the relation is valid for Kr and Xe indicates that it may hold only for molecules or atoms which form strong covalent bonds with CH_3^+ and H^+. Thus, it appears that the bonding mechanism in CH_3^+–Rg complexes sensitively depends on the attached rare gas atom (Rg), whereby the character of the bond changes from mainly electrostatic to mainly covalent as the size of the rare gas increases.

B. CH_3^+–Ar_2 trimer

The photofragmentation spectrum of the CH_3^+–Ar_2 trimer recorded in the CH_3^+–Ar fragment channel is depicted in Fig. 8. As the binding energy of the second Ar atom in CH_3^+–Ar_2 ($\approx 800\ cm^{-1}$) (Ref. 13) is significantly smaller than the vibrational frequencies of CH_3^+, the CH stretching fundamentals of the trimer may be visible in its photodissociation spectrum. Indeed, the ν_3 band of CH_3^+–Ar_2 was observed as a strong transition with an origin at $3152\ cm^{-1}$, i.e. slightly blue shifted from the broad unresolved feature at $3145 \pm 30\ cm^{-1}$ in the CH_3^+–Ar dimer spectrum (associated with $\nu_x + \nu_3 \leftarrow \nu_x$ sequence transitions). The rotational structure of this transition has the form appropriate for a perpendicular band of a prolate symmetric top molecule, with the threefold rotational symmetry supported by the enhanced intensities of the subbands originating from $K = 3n$ $(n > 0)$. However, all Q branch heads appear as doublets separated by approximately $0.5\ cm^{-1}$, indicating that the band is split into two components (Table VII). No such splitting was evident in the spectrum of the CH_3^+–Ar dimer.

The observed splitting in the trimer ν_3 band is most probably due to inversion tunneling. The *ab initio* calculations at the MP2/A level predict for the trimer complex a C_{3v} minimum structure with two nonequivalent C–Ar bonds. The barrier for inversion via the symmetric D_{3h} transition state was calculated to be rather low ($\approx 550\ cm^{-1}$). Consequently, it is conceivable that the two Ar atoms can exchange their roles in an intracluster inversion process. This tunneling motion splits all energy levels of the CH_3^+–Ar_2 complex into two sublevels (inversion doublets)[50] where the vibrational wave function of one component is symmetric (s) and the other is asymmetric (a) with respect to reflection at the ori-

TABLE VII. Positions (in cm^{-1}) of the two Q branches of the $K_a' \leftarrow K_a''$ subbands $(s-s/a-a)$ in the ν_3 photodissociation spectrum of CH_3^+–Ar_2 arising from inversion doubling.[a]

$K_a' \leftarrow K_a''$	$s-s$	$a-a$
$3 \leftarrow 4$	3120.95	3121.44
$2 \leftarrow 3$	3129.66	3130.09
$1 \leftarrow 2$	3138.29	3138.87
$0 \leftarrow 1$	3146.77	3147.23
$1 \leftarrow 0$[b]	3156.24 (3156.05)	3156.56
$2 \leftarrow 1$	3164.10	3164.67
$3 \leftarrow 2$	3172.38	3172.90
$4 \leftarrow 3$	3180.64	3181.17
$5 \leftarrow 4$	3188.75	3189.30

[a]Uncertainty is $0.02\ cm^{-1}$.
[b]This Q branch is split into three components (due to a perturbation).

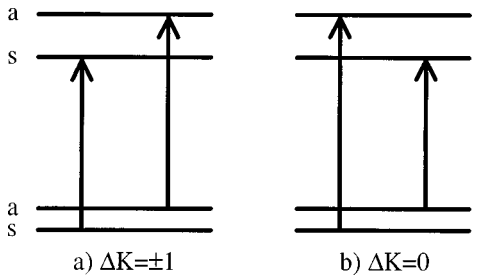

FIG. 9. Allowed transitions between the two inversion tunneling components in a perpendicular (a) and parallel transition (b) of a symmetric top molecule with C_{3v} symmetry.

gin (Fig. 9). In pyramidal XY_3 molecules, like H_3O^+ and NH_3, the inversion splitting significantly depends on the vibrational quantum state of the system.[50] It increases rapidly with the degree of ν_2 excitation (umbrella motion), but changes only slightly upon excitation of the symmetric and asymmetric stretching vibrations (ν_1 and ν_3). The selection rules for a perpendicular transition of a C_{3v} molecule undergoing inversion are such that only the $s-s$ and $a-a$ subbands are allowed [Fig. 9(a)]. Consequently, the observed splitting in the ν_3 transition corresponds to the *difference* in the inversion doubling of the lower (ground) and upper (ν_3) vibrational states. In the case of $CH_3^+-Ar_2$, the separation of the Q branch doublets and their relative intensities implies that the inversion splitting increases by $\approx 0.5\ cm^{-1}$ upon ν_3 excitation. This is in contrast to NH_3 and H_3O^+ where the splitting in the ν_3 state is smaller than in the ground state.

One way to determine the absolute size of the splitting in each of the vibrational states is the direct measurement of the inversion spectrum for the ground state of the complex. However, such an experiment is difficult to perform if an approximate value for the splitting is not available. Alternatively, the magnitude of the splitting can be estimated from the observation of a parallel transition of the complex, which should consist of two subbands separated by the *sum* of the inversion doubling splittings of the lower and upper vibrational states [Fig. 9(b)]. Therefore, the ν_1 transition of the complex was searched for. The transition should be visible as long as the inversion frequency is much lower than the ν_1 frequency. Two extremely weak bands were located at 2981 ± 3 and $2770\pm 2\ cm^{-1}$. Their intensities were almost two orders of magnitude lower than that of the ν_3 band. Despite the poor signal to noise ratio ($\leqslant 2$) their band type could be identified as parallel and perpendicular, respectively. The position of the former band is very close to the prediction for the ν_1 frequency of CH_3^+-Ar derived from the local mode model ($2979\ cm^{-1}$) and the *ab initio* calculation ($2964\ cm^{-1}$, MP2/A). Moreover, the width of this band ($\approx 20\ cm^{-1}$) exceeds the width of other individual bands in the $CH_3^+-Ar_2$ spectrum ($\approx 10\ cm^{-1}$). Consequently, it was concluded that the band centered at $2981\pm 3\ cm^{-1}$ contains both subcomponents ($a-s$ and $s-a$) of the ν_1 transition. From the width of the ν_1 band the inversion splitting of the ground state of the $CH_3^+-Ar_2$ complex can be estimated to be smaller than $7\ cm^{-1}$. This value is based on the assumption that, similar to XY_3 molecules (H_3O^+, NH_3), the splitting does not significantly change upon ν_1 excitation.[50] The magnitude of the ground state splitting can also be estimated from the observed relative intensities of the ν_3 $s-s$ and $a-a$ subbands (1.2 ± 0.1). Assuming that the population of the inversion doublets can be described by the same temperature as the distribution of rotational levels (20–30 K), the splitting can be estimated as $3.5\pm 2\ cm^{-1}$. Finally, it is noted that splittings calculated from the solution of a one-dimensional Schrödinger equation employing a double minimum model potential with a barrier of $300-600\ cm^{-1}$ are of the order of $0.1-5\ cm^{-1}$ (depending on the detailed shape of the potential), compatible with the conclusions derived from the experiment.

The weak perpendicular band at $2770\pm 2\ cm^{-1}$ can tentatively be assigned as the e component ($l=2$) of the $2\nu_4$ overtone of $CH_3^+-Ar_2$, as the ν_4 frequency is around $1400\ cm^{-1}$ for both CH_3^+ and CH_3, and the Ar complexation induced frequency shifts are calculated to be small for this vibration. The alternative scenario that the bands at $2981\ cm^{-1}$ and $2770\ cm^{-1}$ may in fact represent the two subcomponents of the ν_1 transition can be excluded, because the average of the positions of the two bands ($\approx 2880\ cm^{-1}$) is significantly lower than the value expected for the ν_1 frequency of the complex. In addition, the widths and shapes of the bands would not be consistent with such an assignment.

The ν_3 spectrum of $CH_3^+-Ar_2$ exhibits partly resolved rotational structure (Fig. 8). Several P and R branch lines surrounding the $K=1\leftarrow 0$ and $2\leftarrow 1$ Q branches could be identified. In contrast, IR spectra of similar trimeric ionic complexes containing Ar atoms (e.g., ν_1 of HCO^+-Ar_2, ν_3 of $NH_4^+-Ar_2$) (Refs. 31, 32) did not show rotational substructure because of homogeneous and/or inhomogeneous broadening. In the present case the symmetry of the system, the relatively large rotational constants, and the sufficiently long predissociation lifetime made rotational resolution possible. According to the nuclear spin statistics, A_1 rotational levels of an inverting C_{3v} molecule with three equivalent H atoms are missing. Consequently, the $K=1\leftarrow 0$ subband of the ν_3 $s-s$ transition does not contain lines with odd J, while the ν_3 $a-a$ transition lacks lines with even J. The separation between successive P and R branch lines for either $s-s$ or $a-a$ transitions should therefore be of the order of $4B$ for the $K=1\leftarrow 0$ subband and $2B$ for all other subbands in agreement with the experimental observation (see insert in Fig. 8 for $K=1\leftarrow 0$ and $K=2\leftarrow 1$).

A fortuitous circumstance allowed for the resolution of the rotational structure in the $K=1\leftarrow 0$ and $2\leftarrow 1$ subbands. The P and R branch lines originating from the inversion doublets $s-s$ and $a-a$ are nearly coincident, which causes the observed rotational line widths to be significantly broader ($>0.05\ cm^{-1}$) than the laser bandwidth of $0.02\ cm^{-1}$. The absence of any resolved rotational structure in other $K=m\leftarrow n$ subbands may therefore partly arise from the overlap of P and R branch lines of the $s-s$ and $a-a$ transitions. This overlap reduces the precision with which the complex's rotational constants can be determined. From a fit of the $K=1\leftarrow 0$ subband P and R branch lines (28 transitions) to a pseudodiatomic Hamiltonian the follow-

ing molecular constants have been extracted: $B''=0.0358(3)$ cm^{-1}, $D''=2.0(8)\times10^{-6}$ cm^{-1}, $B'=0.0350(3)$ cm^{-1}, and $D'=1.3(8)\times10^{-6}$ cm^{-1}.

The ground state rotational constant of the CH_3^+–Ar_2 trimer corresponds to an Ar–Ar separation of 4.84 ±0.02 Å, which is relatively insensitive to the position of the CH_3^+ unit on the C_{3v} axis. Assuming that the first Ar atom is separated from the carbon atom by the same amount as in the CH_3^+–Ar dimer complex ($R_1=2.02$ Å), the second ligand is estimated to lie $R_2\approx2.8$ Å away from carbon. This implies that the carbon atom moves by as much as $\Delta R\approx0.7$ Å (in the center-of-mass coordinate system) while crossing the inversion barrier, explaining the relatively small magnitude of the inversion splitting. The *ab initio* calculations predict for the two C–Ar separations in the C_{3v} equilibrium geometry of the trimer values of $R_1=2.04$ Å and $R_2=2.88$ Å in close agreement with the values estimated from the experimental spectrum. It is noted that the Ar–Ar separation of 5.24 Å calculated for CH_3^+–Ar_2 in Ref. 13 is not compatible with the present experimental result.

The ν_3 transition of the CH_3^+–Ar_2 is not free from perturbations and interfering sequence bands. Approximately 3 cm^{-1} below each Q branch doublet of the ν_3 band weak unresolved features are observed that are also split into two tunneling components. This sequence band probably originates from one of the intermolecular vibrations of the complex. The most apparent perturbation is mirrored in the significant deviation (≈1 cm^{-1}) of the $K=1\leftarrow0$ subband from the expected position. In addition, the separation between the $s-s$ and $a-a$ Q branches of the $K=1\leftarrow0$ subband is smaller (0.3 cm^{-1}) than for the other $K=n\leftarrow m$ subbands (0.5 cm^{-1}). The nature of the interacting state is unclear at present, possibly it is a combination band of the ν_1 vibration with one of the intermolecular bending modes.

Three weak unresolved transitions of CH_3^+–Ar_2 were identified in the spectral range of the CH stretch overtones between 5950 and 6400 cm^{-1}. From comparison with the dimer spectrum, they can be assigned to $\nu_1+\nu_3$ (6054 ±1 cm^{-1}) and the a_1 and e components of $2\nu_3$ (6224±4 and 6284±2 cm^{-1}). A fit to the local mode model gives following parameters for CH_3^+–Ar_2: $\omega_m=3193(25)$ cm^{-1}, $\chi_m=-50(10)$ cm^{-1}, and $\lambda_m=-54(4)$ cm^{-1}. The addition of the second Ar ligand increases the stretching frequencies of the CH_3^+ core ion further and brings them closer to the corresponding values for the free methyl radical (Table I).

C. Larger clusters CH_3^+–Ar_n ($n=3-8$)

Addition of more Ar atoms into the solvation shell of the CH_3^+–Ar_2 complex results in two principal changes of the photodissociation spectrum in the range of the ν_3 stretching vibration. First, the cluster can now shed more than one ligand upon photoexcitation, because the binding energies for Ar atoms with $n\geqslant2$ are similar (700–800 cm^{-1}) and substantially lower than that for $n=1$.[13] Second, complexes with $n\geqslant3$ are too heavy and, with a few exceptions, too asymmetric to display rotationally resolved spectra at the level of the laser resolution employed here (0.02 cm^{-1}). Thus, the ν_3 photodissociation spectra of CH_3^+–Ar_n clusters

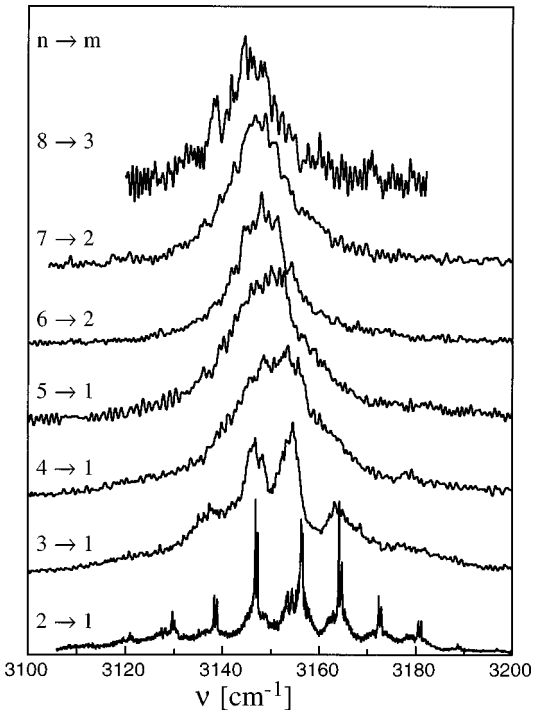

FIG. 10. Photodissociation spectra of the ν_3 band of CH_3^+–Ar_n ($n=2-8$) complexes recorded in the fragment channel CH_3^+–Ar_m.

with $n\geqslant3$ are expected to be structureless, similar to the unresolved CH stretching bands of the Ar_n–HCO^+ ($n=2-12$) (Ref. 32) and Ar_n–CH_5^+ ($n=1-2$) (Ref. 30) cluster series.

Figure 10 compares the ν_3 spectra of the CH_3^+–Ar_n clusters ($n=3-8$) with the corresponding spectrum of the CH_3^+–Ar_2 trimer. The absorptions of the $n=4-8$ clusters are indeed featureless. In contrast, the spectrum of the tetramer ($n=3$) exhibits several distinct and reproducible maxima, which are apparently correlated with the K substructure of the CH_3^+–Ar_2 transition. An equilibrium geometry with two axial and one off-axial Ar atoms[13] cannot give rise to the observed spectral features unless the complex is assumed to be nonrigid. The *ab initio* calculations for the CH_3^+–Ar dimer suggest that the energies for the vertex-bound local minimum and the side-bound transition state are similar (Table III) indicating that the barrier for internal rotation of CH_3^+ around its C_3 axis may be small. If in CH_3^+–Ar_3 this barrier is comparable to or smaller than the A rotational constant of CH_3^+–Ar_2 (≈4–5 cm^{-1}), the latter will undergo (nearly) free internal rotation within the CH_3^+–Ar_3 complex. The observed spectral features would then correspond to $\Delta k_{\rm int}=\pm1$ transitions between different internal rotor states giving rise to a band contour similar to the CH_3^+–Ar_2 trimer band. The presence of two off-axial (i.e., proton-bound) Ar atoms would seem to quench this internal motion, as no such structure is observed in the ν_3 band of CH_3^+–Ar_4.

An alternative CH_3^+–Ar_3 geometry, with the third Ar atom lying on the C_3 axis, would give rise to a spectrum with a course structure similar to that of the CH_3^+–Ar_2 trimer, as both complexes would have comparable A rotational constants. However, considering the inductive interactions of

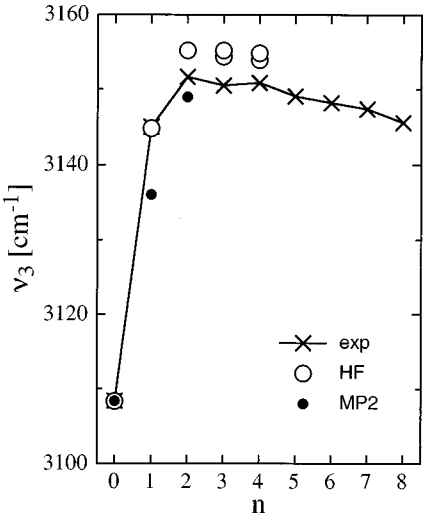

FIG. 11. Comparison of experimental and calculated (HF/A and MP2/B) frequencies of CH_3^+–Ar_n complexes. The HF frequencies for $n=3$ and 4 are based on C_{2v} minima geometries comprising a symmetric D_{3h} trimer and further vertex-bound Ar atoms.

the third Ar atom with the CH_3^+–Ar_2 core the axial site is less favorable than the off-axial proton-bound one, because the charge of the cluster is mainly localized on the CH_3^+ moiety. Therefore, the chain structure is not favored, though the present spectral resolution and the level of the theoretical treatment are not sufficient to definitively determine the $n\geqslant 3$ cluster geometries. In addition, it is not clear whether the inversion motion present in CH_3^+–Ar_2 is quenched by the addition of subsequent Ar atoms.

The ν_3 band origins of the CH_3^+–Ar_n complexes vary in a rather systematic manner with cluster size (Fig. 11, Table VIII). Addition of the first Ar atom to the CH_3^+ ion results in an increase of the ν_3 vibrational frequency from 3108 cm^{-1} in the free methyl cation[20] to around 3145 ± 30 cm^{-1} in the dimer complex. The second Ar atom, attached to the other lobe of the $2p_z$ orbital, induces a smaller incremental frequency shift $\Delta\nu(n)=\nu(n)-\nu(n-1)$, as it is not equivalent to the first Ar atom and features a much weaker intermolecular bond. The direction of the shift $\Delta\nu(2)$ cannot be reliably determined from the experiment due of the large uncertainty in the experimental ν_3 frequency of CH_3^+–Ar. However, the *ab initio* calculations and the local mode model both predict

TABLE VIII. Band centers of the ν_3 vibration of CH_3^+–Ar_n complexes.

n	ν_3 (cm^{-1})
0	3108.3770(57)[a]
1	3145(30)
2	3151.6(5)[b]
3	3150.5(5)
4	3150.9(1.0)
5	3149.1(1.0)
6	3148.2(1.0)
7	3147.4(1.0)
8	3145.6(1.0)

[a]Reference 20.
[b]Average of the $K=1\leftarrow 0$ and $0\leftarrow 1$ subbands.

TABLE IX. Branching ratios[a] for photofragmentation of CH_3^+–Ar_n complexes into the various CH_3^+–Ar_m daughter channels measured at the absorption maxima of the ν_3 transition. Only contributions larger than 0.05 were listed. Clusters with $n=2-4$ fragment exclusively into the $m=1$ channel.

n	$m=1$	$m=2$	$m=3$	$m=4$
5	0.82	0.18		
6		1.00		
7		0.47	0.53	
8			0.45	0.55

[a]Uncertainty is estimated as ± 0.05.

a positive shift (Tables I and V). Addition of further Ar atoms reverses the trend, resulting in incremental shifts to lower frequencies of the CH_3^+–Ar_2 band. The magnitude of the shifts is rather small as the additional intermolecular bonds are weaker than the charge-transfer ones. Negative incremental shifts in the ν_3 frequency are expected for clusters containing off-axial proton-bound Ar atoms ($n\geqslant 3$), as the calculated ν_3 frequency of the vertex-bound dimer is slightly smaller than that of the monomer. Furthermore, off-axial ligands in CH_3^+–Ar_n ($n\geqslant 3$) may push the π-bound ones slightly away from the CH_3^+ core ion, thus destabilizing the axial C–Ar bonds with respect to CH_3^+–Ar_2. This reduces the amount of charge transferred to the $2p_z$ orbital and thus changes the intramolecular frequencies back towards the CH_3^+ values. The fact that the incremental binding energies[13] and frequency shifts are similar for $n\geqslant 3$ may indicate that these Ar atoms occupy equivalent positions in the complex. This observation favors the structures where Ar atoms with $n\geqslant 3$ fill a solvation ring around the CH_3^+–Ar_2 ''rod.'' Unfortunately, there exist no Ar matrix isolation data, making it impossible at this stage to compare the cluster band shifts with the bulk limit.

Size dependent photofragmentation branching ratios can be utilized to roughly estimate the sequential binding energies, $D_0(n)$, of the Ar atoms in the CH_3^+–Ar_n cluster series. As the first Ar atom is relatively strongly bound to the CH_3^+ core, ν_3 excitation of cold CH_3^+–Ar_n clusters cannot lead to CH_3^+ fragments. In contrast, the $2\nu_1$ level lies above the lowest dissociation threshold implying that the binding energy of the dimer lies between 3150 (ν_3) and 5900 cm^{-1} ($2\nu_1$). Clusters with $n=2-4$ fragmented exclusively into CH_3^+–Ar, while for larger ones more than one photodissociation product could be observed (Table IX). For example, the clusters CH_3^+–Ar_7 and CH_3^+–Ar_8 release either 4 or 5 argon atoms with roughly equal probability. The energy absorbed by the cluster ($\nu_3\approx 3150$ cm^{-1}) is used to break the intermolecular bonds by evaporating Ar atoms, and endow the recoiling fragments with a certain amount of internal and kinetic energy. Neglecting the difference in the internal energies of the parent and product complexes, assuming low kinetic energy releases and no polymeric neutral fragments (e.g., Ar_2), several limits for the incremental binding energies can be obtained (Table X). The results are consistent with the experimentally determined enthalpies for sequential CH_3^+–Ar_n clustering reactions.[13]

TABLE X. Incremental binding energies of CH_3^+–Ar_n complexes estimated in the present work compared to available thermochemical data.

n	$D_0(n)$ (cm^{-1})	$-\Delta H_0(n)$ (cm^{-1})[a]
1	$3150<D_0(1)<5900$	3950 ± 700
2	<1050	790 ± 70
3–8	≈700	$\approx680\pm100$

[a]Reference 13.

V. CONCLUSIONS

The structure, energetics and dynamics of the CH_3^+–Ar_n ionic clusters ($n=1-8$) have been investigated by means of IR photofragmentation spectroscopy and *ab initio* calculations. The analysis of the rotationally-resolved spectra of CH stretching overtones of CH_3^+–Ar revealed that the dimer is a strongly bound complex ($D_0\approx0.5$ eV) with a pyramidal C_{3v} structure and an intermolecular separation of the order of 2.0 Å. The Ar atom serves as electron donor for the empty electrophilic $2p_z$ orbital of CH_3^+ and the resulting charge transfer causes the CH_3^+ moiety to become pyramidal upon formation of the π-bound complex. The CH_3^+–Ar_2 trimer complex is characterized by a C_{3v} equilibrium structure with an Ar–Ar separation of 4.84 Å. The two intermolecular bonds are not equivalent and the two Ar atoms exchange their roles by an intracluster inversion tunneling motion of the CH_3^+ moiety. The D_{3h} structure, previously predicted as the global minimum,[13] is in fact a transition state for the inversion motion between two equivalent C_{3v} global minima. The double-minimum potential found for $Ar\cdots CH_3^+\cdots Ar$ lends spectroscopic evidence to previous suggestions that degenerate nucleophilic S_N2 reactions of the type $X^-+CH_3X\rightarrow XCH_3+X^-$ (where X is for example a halogen atom) may occur along a reaction coordinate with a symmetric double minimum potential.[56,57] The stretching frequencies of the CH_3^+ moiety shift significantly towards the respective values of the CH_3 radical upon attachment of the first and second Ar atom. This is interpreted to result from an increase of the electron density in the $2p_z$ orbital of CH_3^+ due to charge transfer from the axial argon atoms. Additional Ar ligands ($n\geqslant3$) are weakly attached to the trimer core and have little influence on the CH_3^+–Ar_2 nucleation center. Vibrational frequency shifts suggest that they fill a solvation ring around the CH_3^+–Ar_2 ''rod.'' Experimental and theoretical work on CH_3^+–Ne_n and CH_3^+–He_n is in progress to study the properties of this class of π-bound complexes as a function of the intermolecular bond strength.

ACKNOWLEDGMENTS

This study is part of the project No. 20-49104.96 of the Swiss National Science Foundation. We would like to thank V. Špirko for calculating the frequencies of the CH stretching overtones of CH_3^+ and CH_3 using the nonrigid inverter model, and J.M.L. Martin for useful discussions concerning the force field of the CH_3^+ ion.

[1] G. A. Olah and P. R. Schleyer, *Carbonium Ions I* (Wiley, New York, 1968).
[2] G. A. Olah and P. R. Schleyer, *Carbonium Ions V* (Wiley, New York, 1976).
[3] D. Smith, Chem. Rev. **92**, 1473 (1992).
[4] H. Suzuki, Prog. Theor. Phys. **62**, 936 (1979).
[5] D. Smith, Philos. Trans. R. Soc. London, Ser. A **324**, 257 (1988).
[6] E. W. Kaiser, J. Phys. Chem. **94**, 4493 (1990).
[7] U. Meier and K. Kohse-Höinghaus, Chem. Phys. Lett. **142**, 498 (1987).
[8] J. Pacansky, W. Koch, and M. D. Miller, J. Am. Chem. Soc. **113**, 317 (1991).
[9] T. Oka, Philos. Trans. R. Soc. London, Ser. A **324**, 81 (1988).
[10] M. Venugoplan, U. K. Roychowdhury, K. Chan, and M. L. Pool, in *Plasma Chemistry II* (Springer, Berlin, 1980), Vol. 90, p. 1.
[11] K. Morokuma, J. Chem. Phys. **94**, 4858 (1991).
[12] N. E. Triggs, M. Zahedi, J. W. Nibler, P. DeBarber, and J. J. Valentini, J. Chem. Phys. **96**, 1822 (1992).
[13] K. Hiraoka, I. Kudaka, and S. Yamabe, Chem. Phys. Lett. **178**, 103 (1991).
[14] K. Hiraoka, J. Katsuragawa, T. Sugiyama, A. Minamitsu, S. Yamabe, and H. Kouno, Chem. Phys. Lett. **271**, 302 (1997).
[15] L. F. Phillips, J. Phys. Chem. **94**, 5265 (1990).
[16] D. M. Sonnenfroh and J. M. Farrar, J. Chem. Phys. **85**, 7167 (1986).
[17] R. Bucci, F. Grandinetti, A. Filippi, G. Laguzzi, G. Occhiucci, and M. Speranza, J. Am. Chem. Soc. **113**, 4550 (1991).
[18] W. T. Huntress, Astrophys. J., Suppl. **33**, 495 (1977).
[19] S. Mark, C. Schellhammer, G. Niedner-Schatteburg, and D. Gerlich, J. Phys. Chem. **99**, 15587 (1995).
[20] M. W. Crofton, M.-F. Jagod, B. D. Rehfuss, W. A. Kreiner, and T. Oka, J. Chem. Phys. **88**, 666 (1988).
[21] T. Koenig, T. Balle, and W. Snell, J. Am. Chem. Soc. **97**, 662 (1975).
[22] J. Dyke, N. Jonathan, E. Lee, and A. Morris, J. Chem. Soc., Faraday Trans. 2 **72**, 1385 (1976).
[23] C. Yamada and E. Hirota, J. Chem. Phys. **78**, 669 (1983).
[24] T. B. McMahon, T. Heinis, G. Nicol, J. K. Hovey, and P. Kebarle, J. Am. Chem. Soc. **110**, 7591 (1988).
[25] G. E. Scuseria, Nature (London) **366**, 512 (1993).
[26] D. Marx and M. Parrinello, Nature (London) **375**, 216 (1995).
[27] M. Okumura, L. I. Yeh, and Y. T. Lee, J. Chem. Phys. **83**, 3705 (1985).
[28] O. Dopfer, S. A. Nizkorodov, M. Meuwly, E. J. Bieske, and J. P. Maier, Chem. Phys. Lett. **260**, 545 (1996).
[29] S. A. Nizkorodov, J. P. Maier, and E. J. Bieske, J. Chem. Phys. **103**, 1297 (1995).
[30] D. W. Boo and Y. T. Lee, Int. J. Mass Spectrom. Ion Processes **159**, 209 (1996).
[31] O. Dopfer, S. A. Nizkorodov, M. Meuwly, E. J. Bieske, and J. P. Maier, Int. J. Mass Spectrom. Ion Processes **167-168**, 637 (1997).
[32] S. A. Nizkorodov, O. Dopfer, T. Ruchti, M. Meuwly, J. P. Maier, and E. J. Bieske, J. Phys. Chem. **99**, 17118 (1995).
[33] S. G. Westre, X. Liu, J. D. Getty, and P. B. Kelly, J. Chem. Phys. **95**, 8793 (1991).
[34] P. B. Kelly and S. G. Westre, Chem. Phys. Lett. **151**, 253 (1988).
[35] T. J. Sears, J. M. Frye, V. Spirko, and W. P. Kraemer, J. Chem. Phys. **90**, 2125 (1989).
[36] V. Spirko and P. R. Bunker, J. Mol. Spectrosc. **95**, 381 (1982).
[37] V. Spirko and W. P. Kraemer, J. Mol. Spectrosc. **153**, 285 (1992).
[38] V. Spirko, J. Mol. Spectrosc. **101**, 30 (1983).
[39] M. W. Crofton, W. A. Kreiner, M.-F. Jagod, B. D. Rehfuss, and T. Oka, J. Chem. Phys. **83**, 3702 (1985).
[40] W. P. Kraemer and V. Spirko, J. Mol. Spectrosc. **149**, 235 (1991).
[41] V. Spirko (private communication, 1997).
[42] E. J. Bieske, S. A. Nizkorodov, F. R. Bennett, and J. P. Maier, J. Chem. Phys. **102**, 5152 (1995).
[43] E. J. Bieske, J. Chem. Soc. Faraday Trans. **91**, 1 (1995).
[44] G. Guelachvili and K. N. Rao, *Handbook of Infrared Standards* (Academic, London, 1993).
[45] M. J. Frisch, G. W. Trucks, H. B. Schlegel, P. M. W. Gill, B. G. Johnson, M. A. Robb, J. R. Cheeseman, T. Keith, G. A. Petersson, J. A. Montgomery, K. Raghavachari, M. A. Al-Laham, V. G. Zakrzewski, J. V. Ortiz, J. B. Foresman, J. Cioslowski, B. B. Stefanov, A. Nanayakkara, M. Challacombe, C. Y. Peng, P. Y. Ayala, W. Chen, M. W. Wong, J. L. Andres, E. S. Replogle, R. Gomperts, R. L. Martin, D. J. Fox, J. S. Binkley, D. J. Defrees, J. Baker, J. P. Stewart, M. Head-Gordon, C. Gonzales, and J. A. Pople, Gaussian, Inc., Pittsburgh, Pennsylvania, 1995.
[46] Extensible Computational Chemistry Environmental Basis Set Data Base, Version 10 (1996).

[47] S. F. Boys and F. Bernardi, Mol. Phys. **19**, 553 (1970).
[48] G. Chalasinski and M. M. Szczesniak, Chem. Rev. **94**, 1 (1994).
[49] T. Amano, P. F. Bernath, C. Yamada, Y. Endo, and E. Hirota, J. Chem. Phys. **77**, 5284 (1982).
[50] G. Herzberg, *Molecular Spectra and Molecular Structure. II. Infrared and Raman Spectra of Polyatomic Molecules* (Krieger, Malabar, 1991).
[51] S. A. Nizkorodov, Y. Spinelli, E. J. Bieske, J. P. Maier, and O. Dopfer, Chem. Phys. Lett. **265**, 303 (1997).
[52] P. Jensen, S. Brodersen, and G. Guelachvili, J. Mol. Spectrosc. **88**, 378 (1981).
[53] H. Okabe, *Photochemistry of Small Molecules* (Wiley, New York, 1978).
[54] J. K. Hovey and T. B. McMahon, J. Phys. Chem. **91**, 4560 (1987).
[55] A. J. R. Heck, L. J. d. Koning, and N. M. M. Nibbering, J. Phys. Chem. **96**, 8870 (1992).
[56] W. N. Olmstead and J. I. Brauman, J. Am. Chem. Soc. **99**, 4219 (1977).
[57] M. J. Pellerite and J. I. Brauman, J. Am. Chem. Soc. **102**, 5993 (1980).
[58] M. Zahedi, J. A. Harrison, and J. W. Nibler, J. Chem. Phys. **100**, 4043 (1994).
[59] C. Yamada, E. Hirota, and K. Kawaguchi, J. Chem. Phys. **75**, 5256 (1981).
[60] S. Davis, D. T. Anderson, G. Duxbury, and D. J. Nesbitt, J. Chem. Phys. **107**, 5661 (1997).
[61] A. Snelson, J. Phys. Chem. **74**, 537 (1970).